An Adjoint Method for Channel Localization

Steven J. Cox
Computational and Applied Mathematics, MS 134
Rice University, 6100 Main, Houston, TX 77006

Abstract: Single cells learn by tuning their synaptic conductances and redistributing their excitable machinery. To reveal its learning rules one must therefore know how the cell remaps its ion channels in response to physiological stimuli. We here develop an adjoint approach for discerning the nonuniform distribution of a given channel type from knowledge of the time course of membrane potential at two distinct locations following a prescribed injection of current.

1. Introduction

Individual cells learn both by tuning their synaptic conductances and by modulating their intrinsic excitability, Daoudal & Debanne (2003) and Xu *et al.* (2005). By intrinsic excitability we mean not only whether it is a burster or spiker and at what rate it fires but rather the type and location of each of its membrane conductances. For example, in hippocampal pyramidal cells there exist nonuniform distributions of channels responsible for the persistent sodium current, the low–threshold T-type calcium current, the transient A-type potassium current and the hyperpolarization activated current, I_h, with each exerting demonstrable molding of synaptic input, Hoffman *et al.* (1997), Magee (1999) for review see Reyes (2001). Our intent here is to develop a minimally invasive means for localizing channels and monitoring the stimulus driven modulation of their densities. We begin with a short survey of the competing technologies for charting ion channel distribution.

Early maps of sodium and calcium channel distributions in Purkinje cells were constructed with optical probes by Sugimori *et al.* (1986) and Ross & Werman (1986) respectively. Sabatini & Svoboda (2000) have since refined this practice. Lorincz *et al.* (2002) immunogold stained the HCN1 subunit of the hyperpolarization activated nonselective cation channel associated with the I_h current in rat brain and counted, under the electron microscope, the membrane-bound gold particles in pyramidal cells. Their findings are dramatic - namely, a 60-fold increase in HCN1 density from somatic to distal apical dendritic membrane. This is without doubt the most accurate of the available methods. Unfortunately it is also the most invasive. Earlier such uses of immunocytochemistry have indicated nonuniformities, Elliott *et al.* (1995), with regard to variation in calcium channel type, but in not nearly so quantitative a manner.

Hoffman *et al.* (1997) recorded potassium currents in cell-attached patch clamp mode along the somadendritic axis of 57 CA1 pyramidal cells in hippocampal brain slices. They found a 6-fold increase in the peak current density of A-type K^+ channels per patch from the soma to the distal dendrites. They also found a 12 mV leftward shift in the channel's associated steady-state activation function as one traveled from the soma into the apical tree. They argue that in light of the fairly uniform distribution of transient Na^+ channels it is this increase in dendritic A-type K^+ channel that dampens the excitability of the apical tree and so Migliore *et al.* (1999) is responsible for the attenuation of back propagating action potentials. Regarding sodium channels, although Colbert *et al.* (1997) and Mickus *et*

al. (1999) found relatively constant density throughout the cell they did detect a difference in inactivation properties between the soma and dendrites. By the same method, and also in CA1 pyramidal neurons in brain slices, Magee (1998) found more than a 6-fold increase in h-current density. He argued in Magee (1999) that this nonuniformity counterbalances the dendritic filter seen by distal synapses and so renders somatic temporal summation independent of synaptic location. These cell–attached and excised–patch methods however produce very small currents and suffer from large variability in patch area and uncertainty regarding the number of channels per patch. These shortcomings have been overcome with the whole–cell traveling voltage clamp of Schaefer *et al.* (2003) in the mapping of potassium channel distribution in neocortical pyramidal cells. Although this boosted the currents and signal–to–noise ratio it exposed them to the lack of space–clamp. They correct for this lack via an ingenious, though laborious, computational fitting procedure, that, at present, is limited to nonregenerative currents. An alternate means for thwarting the lack of space clamp is to simultaneously record the potential at multiple sites, as done by Stuart & Spruston (1998). They hypothesized parametric nonuniform expressions for leakage and h conductances and determined their free parameters, with limited success, by fitting simulated potentials to membrane potentials, simultaneously measured at the soma and one dendritic site, with patch electrodes in neocortical pyramidal cells.

We argue below that, in the context of determining nonuniformities from such dual potential recordings, misfit minimization can be made substantially faster and simultaneously more accurate by adopting a gradient search scheme. One reason why this technique has not received previous application is the apparent difficulty in computing the gradient of the misfit with respect to an unknown nonuniformity. We show that the adjoint, or Lagrange multiplier, method provides a fast and intuitive means for computing the gradient. We then demonstrate the superiority of gradient search to direct search on simulated data for both the passive and active problems of Stuart & Spruston (1998). We provide full implementation details in the passive case and limit our exposition of the active case to the derivation of the associated adjoint equation. Such dual potential data has been exploited in the past Cox & Griffith (2001) and Cox & Li (2001) to estimate uniform, or effective, densities and kinetic functionals.

2. **The Nonuniform Passive Cable**

Let us recall the setting of Stuart & Spruston (1998). At its simplest, one has a cable of length ℓ and radius a with axial resistivity R_i, membrane capacitance C_m and **nonuniform** leakage conductance $G_l(x)$ with associated leakage potential E_l. The axial resistivity appears most naturally in terms of the axial conductance $G_i \equiv a/(2R_i)$. If v denotes the transmembrane potential then the axial and membrane currents balance when v obeys the **cable equation**

$$G_i v_{xx}(x,t) = C_m v_t(x,t) + G_l(x)(v(x,t) - E_l) \tag{2.1}$$

for $0 < x < \ell$ and $t > 0$. The cable is initially at rest

$$v(x,0) = E_l, \qquad 0 < x < \ell \tag{2.2}$$

and the right end is sealed while the left receives a subthreshold current pulse, i_0, i.e.,

$$v_x(0,t) = -\frac{R_i}{\pi a^2} i_0(t) \quad \text{and} \quad v_x(\ell,t) = 0, \qquad 0 < t. \tag{2.3}$$

Stuart and Spruston sought to determine G_l through knowledge of the time course of the potential at the soma and at the dendritic location, x_1. More precisely, via measurement of

$$v(0,t) = v_0^e(t) \quad \text{and} \quad v(x_1,t) = v_1^e(t) \tag{2.4}$$

over some interval $t \in [0,T]$. Regarding uniqueness, Pierce (1979) appears to be the first to have proven that there is at most one G_l for which the full problem, (2.1)–(2.4), is consistent. Where Pierce assumed only Hölder continuity of G_l, Stuart and Spruston confined themselves to nonuniformities of the form

$$\frac{1}{G_l(x)} = R_m(x) = b + \frac{a-b}{1+\exp((h-x)/s)} \tag{2.5}$$

and sought the vector of free parameters, $G = \{a, b, h, s\}$, that best fit their data, (2.4), recorded in the presence of the h-current blocker, CsCl. They then used the neuro-simulator NEURON Hines & Carnevale (1997) to specify a parameter set and solve the cable equation (2.1) subject to the boundary conditions (2.3). The simulated solution is deemed $v(x,t;G)$ and PRAXIS, the principal axis method of Brent (2002) is used to minimize the misfit between experiment and simulation over the time interval $[0,T]$. More precisely, they solved

$$\min_G \Phi(G) \tag{2.6}$$

where Φ is the misfit function

$$\Phi(G) \equiv \frac{1}{2}\int_0^T \{|v_0^e(t) - v(0,t;G)|^2 + |v_1^e(t) - v(x_1,t;G)|^2\}\, dt. \tag{2.7}$$

Stuart and Spruston reported that "The fits with nonuniform R_m models, however, were still imperfect (particularly during the falling phase of the short-pulse responses), which may be because of the way nonuniform R_m was incorporated into these models. Other nonuniform functions were tried (e.g., step, linear) but were either worse or did not improve the fits." Hence it makes sense to offer the minimization procedure as much freedom as possible. The difficulty here however is that as the number of free parameters increases so too does the computational cost of finding the best fit. This is especially true of direct search procedures such as PRAXIS. One typically only uses such procedures, rather than gradient descent methods, when the gradient of the misfit functional either does not exist or is too expensive to compute. As neither of these pertains let us now develop the gradient of (2.7) and put it to good use.

In what follows the candidate leakage conductance, G, is assumed only to be a bounded function of position, x, along the fiber. We proceed by adjoining the cable equation, (2.1),

to the (liberated) objective function, (2.7), via an adjoint variable, V. That is, we define and study the **Lagrangian**

$$L(G,v,V) = \frac{1}{2}\int_0^T \{|v_0^e(t) - v(0,t)|^2 + |v_1^e(t) - v(x_1,t)|^2\}\,dt$$
$$+ R_i \int_0^T \int_0^\ell \{C_m v_t(x,t) - G_i v_{xx}(x,t) + G(x)(v(x,t) - E_l)\}V(x,t)\,dx\,dt,$$

where v is liberated in the sense that it is assumed only to satisfy the boundary, (2.3), and initial, (2.2), conditions. The leading R_i above was chosen only so that V too will be in units of mV. The formal connection between L and Φ,

$$\Phi(G) = \min_v \max_V L(G,v,V)$$

suggests that the gradient of Φ is simply the gradient of L with respect to G at the saddle point of $L(G,\cdot,\cdot)$. That is, the gradient of Φ at G in the direction $\tilde{G}$ is

$$\langle \partial\Phi(G), \tilde{G}\rangle = \langle \partial_G L(G,v,V), \tilde{G}\rangle = R_i \int_0^T \int_0^\ell (v(x,t) - E_l)V(x,t)\tilde{G}(x)\,dx\,dt \tag{2.8}$$

so long as v and V are critical points of L at G, i.e.,

$$\partial_v L(G,v,V) = \partial_V L(G,v,V) = 0. \tag{2.9}$$

The tools necessary for a rigorous derivation of (2.8) are developed in Lions (1971).

We recognize the latter equality in (2.9) as a restatement of the cable equation, i.e., v should coincide with $v(\cdot,\cdot;G)$. The former equality in (2.9) will lead to a new cable equation for V that will permit us to efficiently compute (2.8). More precisely, the gradient of L with respect to v in the direction $\tilde{v}$ is

$$\langle \partial_v L(G,v,V), \tilde{v}\rangle = \lim_{\varepsilon\to 0} \frac{L(G,v+\varepsilon\tilde{v},V) - L(G,v,V)}{\varepsilon}$$
$$= \int_0^T \{(v(0,t) - v_0^e(t))\tilde{v}(0,t) + (v(x_1,t) - v_1^e(t))\tilde{v}(x_1,t)\}\,dt$$
$$+ R_i \int_0^T \int_0^\ell \{C_m \tilde{v}_t - G_i \tilde{v}_{xx} + G(x)\tilde{v}\}V\,dx\,dt,$$

where, in order that $v+\varepsilon\tilde{v}$ satisfy the same initial and boundary conditions as v, we require

$$\tilde{v}_x(0,t) = \tilde{v}_x(\ell,t) = \tilde{v}(x,0) = 0.$$

With this we now integrate the double integral by parts and find

$$\langle \partial_v L(G,v,V), \tilde{v}\rangle = \int_0^T \{v(0,t) - v_0^e(t) - (a/2)V_x(0,t)\}\tilde{v}(0,t)\,dt$$
$$+ (a/2)\int_0^T V_x(\ell,t)\tilde{v}(\ell,t)\,dt + R_i C_m \int_0^\ell \tilde{v}(x,T)V(x,T)\,dx$$
$$+ R_i \int_0^T \int_0^\ell \{-C_m V_t - G_i V_{xx} + G(x)V + \delta(x-x_1)(v - v_1^e(t))/R_i\}\tilde{v}\,dx\,dt.$$

In order for this to vanish, as required by (2.9), in every direction $\tilde{v}$, we see that V must satisfy the **Adjoint Cable Equation**

$$-C_m V_t - G_i V_{xx} + G(x)V = \delta(x - x_1)(v_1^e(t) - v(x_1, t; G))/R_i \tag{2.10}$$

$$V(x, T) = 0 \tag{2.11}$$

$$(a/2)V_x(0, t) = v(0, t; G) - v_0^e(t) \tag{2.12}$$

$$(a/2)V_x(\ell, t) = 0. \tag{2.13}$$

We wish to point out that this has much in common with our original cable equation (2.1)–(2.3). While we solve the latter forward in time from $t = 0$ with experimentally provided current stimulus at the spatial boundary we solve the adjoint cable equation backward in time from $t = T$ with boundary and internal currents dictated by the mismatch between the experimental and simulated potentials. In particular, if this mismatch is zero then V itself will be zero and hence, recalling (2.8), so too will be the gradient of Φ. This is precisely the objective of a gradient descent method – to minimize Φ by descending to a critical point.

We now address the practical implementation of these ideas. We solve the cable problem, (2.1)–(2.3), via backward Euler in time and finite elements in space and we solve the adjoint cable equation, (2.10)–(2.13), via forward Euler in time and finite elements in space. In particular we partition space and time according to

$$[0, h, 2h, \ldots, (N_x - 1)h = \ell] \quad \text{and} \quad [0, \tau, 2\tau, \ldots, (N_t - 1)\tau = T]$$

and assume the minimum regularity of $v(\cdot, t)$, $V(\cdot, t)$ and G_l commensurate with the weak forms of the two cable problems. Namely, that $v(\cdot, t)$ and $V(\cdot, t)$ are each piecewise linear while G_l is piecewise constant. More precisely,

$$v(x, (j-1)\tau) = \sum_{i=1}^{N_x} \mathtt{v}_{i,j} H_i(x) \qquad V(x, (j-1)\tau) = \sum_{i=1}^{N_x} \mathtt{V}_{i,j} H_i(x)$$

$$G_l(x) = \sum_{i=1}^{N_x - 1} \mathtt{Gl}_i \chi_i(x),$$

where

$$H_i(x) = \begin{cases} 1 - |x - (i-1)h|/h & \text{if } (i-2)h < x < ih \\ 0 & \text{if otherwise} \end{cases}$$

$$\chi_i(x) = \begin{cases} 1 & \text{if } (i-1)h < x < ih \\ 0 & \text{otherwise.} \end{cases}$$

On substituting these representations into weak versions of our respective cable equations we arrive at a linear system that permits us to march forward from $\mathtt{v}_{:,j-1}$ to $\mathtt{v}_{:,j}$, namely

$$\begin{aligned} (\mathtt{M} + \mathtt{K} + \mathtt{L})\mathtt{v}_{:,j+1} &= \mathtt{M}\mathtt{v}_{:,j} + \mathtt{b} + i_0((j+1)\tau)\mathtt{e}_1/(2\pi a) \\ \mathtt{v}_{:,1} &= E_l \mathtt{1} \end{aligned} \tag{2.14}$$

and a linear system that permits us to march backward from $\mathtt{V}_{:,j+1}$ to $\mathtt{V}_{:,j}$, namely

$$\begin{aligned}(\mathtt{M}+\mathtt{K}+\mathtt{L})\mathtt{V}_{:,j} &= \mathtt{M}\mathtt{V}_{:,j+1} + (v_0^e(j\tau) - \mathtt{v}_{1,j})\mathtt{e}_1/R_i + (v_1^e(j\tau) - \mathtt{v}_{d,j})\mathtt{e}_d/R_i \\ \mathtt{V}_{:,N_t} &= \mathtt{0},\end{aligned} \tag{2.15}$$

where $\mathtt{e}_k$ is the coordinate vector of zeros except for a 1 in the kth entry, where $d = x_1/h$ is the index of the dendritic recording electrode and where $\mathtt{M}$, $\mathtt{K}$, and $\mathtt{L}$ are the symmetric tridiagonal matrices

$$\begin{aligned}\mathtt{M}(i,i+1) &= \frac{C_m h}{6\tau} \qquad \mathtt{M}(i,i) = \frac{C_m h}{6\tau}\begin{cases}2 & \text{if } i=1 \quad \text{or} \quad i=N_x\\ 4 & \text{otherwise}\end{cases}\\ \mathtt{K}(i,i+1) &= -\frac{G_i}{h} \qquad \mathtt{K}(i,i) = \frac{G_i}{h}\begin{cases}1 & \text{if } i=1 \quad \text{or} \quad i=N_x\\ 2 & \text{otherwise}\end{cases}\\ \mathtt{L}(i,i+1) &= \frac{h}{6}\mathtt{Gl}_i \qquad \mathtt{L}(i,i) = \frac{h}{6}\begin{cases}2\mathtt{Gl}_1 & \text{if } i=1\\ 2\mathtt{Gl}_{N_x-1} & \text{if } i=N_x\\ 2(\mathtt{Gl}_{i-1}+\mathtt{Gl}_i) & \text{otherwise}\end{cases}\end{aligned}$$

and

$$\mathtt{b}_i = \frac{E_l h}{2}\begin{cases}\mathtt{Gl}_1 & \text{if } i=1\\ \mathtt{Gl}_{N_x-1} & \text{if } i=N_x\\ \mathtt{Gl}_{i-1}+\mathtt{Gl}_i & \text{otherwise.}\end{cases}$$

To solve (2.14) and (2.15) we form and factor $\mathtt{M}+\mathtt{K}+\mathtt{L}$ only once, at the outset. The only burden is that we must store the full $\mathtt{v}$ and $\mathtt{V}$ in preparation for the gradient computation. In terms of the finite element discretization, the gradient, (2.8), takes the concrete form

$$\frac{\partial\Phi(\mathtt{Gl})}{\partial\mathtt{Gl}_i} = \frac{R_i h\tau}{6}\sum_{j=1}^{N_t}\{(2\mathtt{v}_{i,j} - 3E_l + \mathtt{v}_{i+1,j})\mathtt{V}_{i,j} + (2\mathtt{v}_{i+1,j} - 3E_l + \mathtt{v}_{i,j})\mathtt{V}_{i+1,j}.\} \tag{2.16}$$

In practice, in order to accurately compute the synthetic potentials, N_x must be large, i.e., we require a large number of compartments. As the cost of minimization of Φ typically grows with the number of free parameters in G_l it seems wise to only permit G_l to vary on a subset of the $N_x - 1$ compartments and to increase the size of this subset only when dissatisfied with the current fit. One simple way to do this is to lump the small compartments into modules of m compartments. More precisely, we write

$$G_l(x) = \sum_{i=1}^{(N_x-1)/m} \mathtt{Gl}_i\Xi_i(x) \quad \text{where} \quad \Xi_i(x) = \begin{cases}1 & \text{if } (i-1)mh < x < imh,\\ 0 & \text{otherwise.}\end{cases} \tag{2.17}$$

In this way one can generate a heirarchy of leak profiles by using the G_l obtained at level m as the starting guess at level $m-1$.

We have coded the requisite steps in Matlab and invoked its optimization toolbox in the minimization of Φ. In particular, we compare the response of the gradient based unconstrained minimization routine, `fminunc`, with that of the Nelder–Mead (PRAXIS like) direct search routine, `fminsearch`. When the former is invoked without a user supplied

gradient the gradient is approximated via brute–force finite differencing. Both `fminunc` and `fminsearch` support a number of options. We use the default options except for setting `tolfun=1e-5` throughout and `largescale=off` when using `fminunc`.

We compare these methods on the synthetic fiber with geometry, passive parameters, stimulus, nonuniform leak term and discretization parameters listed below

$$\begin{aligned} \ell = 1\ mm, \quad a = 2\,\mu m, \quad E_l = -65\ mV \\ C_m = 1\ \mu F/cm^2, \quad R_i = 60\ \Omega cm, \quad x_1 = 0.75\ mm \\ i_0(t) = 0.3\max(t-1,0)\exp(-\max(t-1,0)/2)\ nA, \\ G_l(x) = 0.2 + 0.2/(1+\exp((\ell/2-x)/0.01))\ mS/cm^2 \\ h = 0.025\ mm, \quad \tau = 0.02\ ms. \end{aligned} \tag{2.18}$$

This value of h corresponds to $N_x = 41$ compartments. Given the gradual slope of G_l we have lumped these into groups of $m = 5$ with regard to (2.17). We also present the results of a typical recovery of a nonmonotone leakage term, in particular

$$G_l(x) = 0.1(2 + \cos(2\pi x/\ell))\ mS/cm^2. \tag{2.19}$$

In each case, as a nod to measurement error, we sully the computed potentials, v_0^e and v_1^e,

$$v_j^e(t) = v_j^e(t)(1 + \omega(t))$$

where $\omega(t)$ is drawn from a normal distribution with mean zero and a standard deviation of 0.0004.

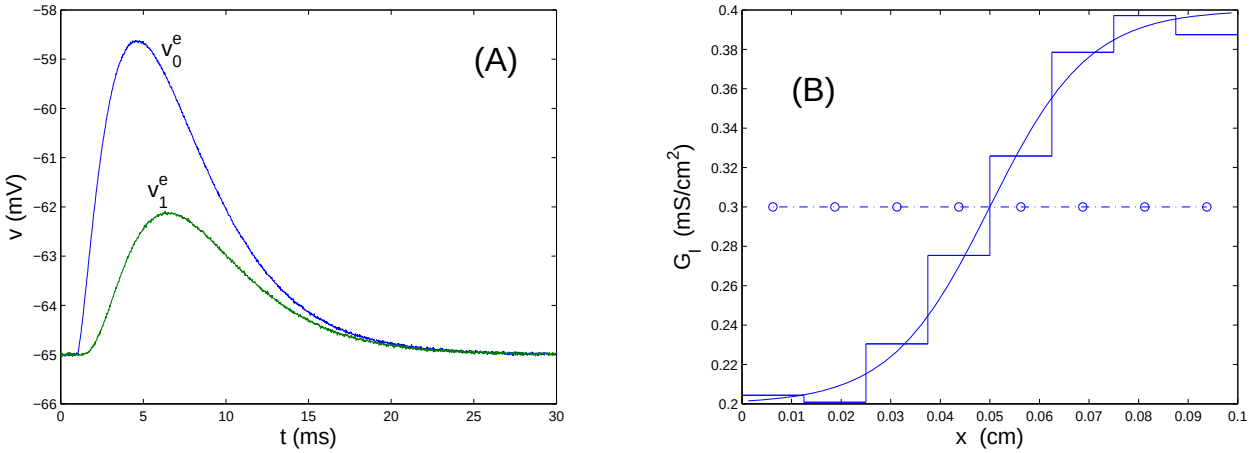

Figure 1. Reconstruction of a nonuniform leakage conductance for the passive cell and stimulus described by (2.18). (A) The 'data', i.e., the simulated potential at 0 and x_1. (B) Exact, initial (o) and recovered (staircase) leakage conductance using the gradient search routine `fminunc`.

In arriving at figure 1(B) `fminunc` required 20 iterations which in turn required a total of 24 function evaluations. Each function evaluation required the solution of the cable equation, (2.14), the adjoint cable equation, (2.15), and the assembly of the gradient,

(2.16). By comparison, when we ran `fminunc` without supplying the gradient it required 33 iterations and 333 function evaluations. In this case each function evaluation required only the solution of the cable equation, (2.14). So, although each evaluation was twice as fast we required almost 14 times as many of them. Regarding `fminsearch`, we typically terminated the search after 500 iterations and some 730 function evaluations, prior to meeting the default stopping criteria and far from the 'true' conductance profile.

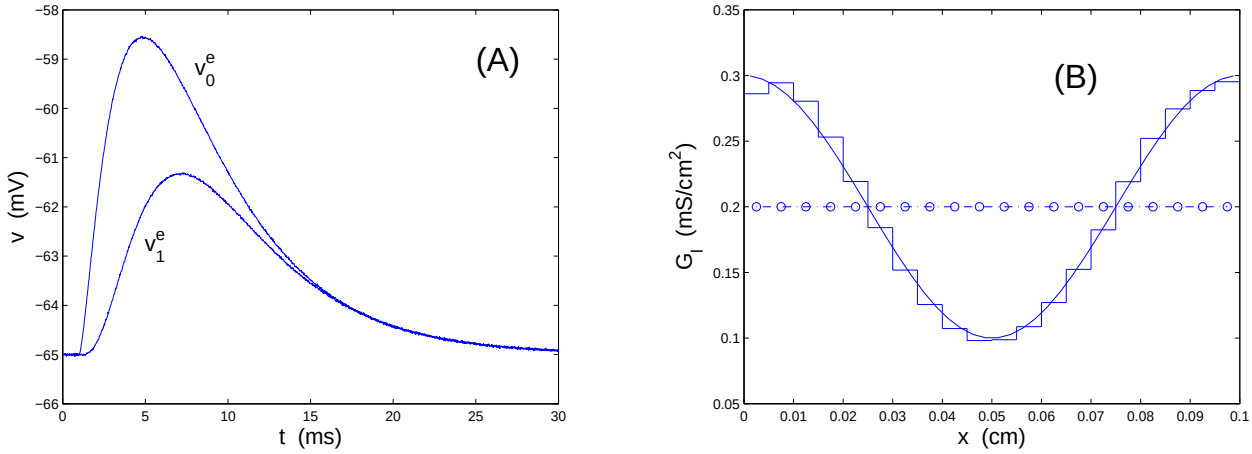

Figure 2. Reconstruction of the nonmonotone leak term, (2.19). All other parameters are as described in (2.18). In pursuing a term with greater variability we have also shrunk m to 2 from 5. (A) The associated potentials. (B) Exact, initial (o) and recovered (staircase) leakage conductance using the gradient search routine `fminunc`.

In reconstructing (2.19), see fig. 2, the gradient search converged in 50 iterations and took 53 full function evaluations. Withholding our gradient resulted in 50 iterations and 1155 half function evaluations while the 500 permitted iterations of `fminsearch` cost 672 half function evaluations and yet was still far from the desired conductance profile. As the true cost is typically clock time we now contrast (in Table 1) the time required of the 3 methods as the problem size increases.

mod	**fminunc**	**fminunc, no grad**	**fminsearch**
5	6.7	10.1	135
10	7.0	15.1	135
20	8.4	26.6	135
40	8.3	55.1	135

Table 1. Comparison of the performance of three misfit minimization schemes for the cell described by (2.18) in the absence of measurement noise, i.e., $\omega = 0$. The first column denotes the number of modules ($mod = (N_x - 1)/m$) on which G_l is permitted to vary. The remaining columns record the time, in seconds (on a Windows machine with an AMD Athlon 4), that `fminunc`, with and without our user supplied gradient, and `fminsearch` required to recover G_l. The latter routine indeed consistently hit the ceiling of 500 iterations. The cost of the gradient routine grew linearly with problem size when invoked without the user supplied gradient. Its cost with the gradient is cheap and essentially independent of problem size.

We stress that the examples presented here are representative and not indicative of hidden constraints or assumptions. For example one may commence from an aribitrary starting guess and the sought after G_l need not be even or odd. Regarding the choice of starting guess, our method is merely an acceleration of gradient search and as such is not immune from stalling at suboptimal loca minima.

Regarding further extensions and limitations it is a simple matter to work on tapered fully active cables, as we shall soon demonstrate. It is not a simple matter to move to branched cells, for in that case knowledge of the potential at two sites does not uniquely determine the desired conductance profile. Following Belishev (2004) it suffices to know the potential somewhere on each terminal branch. As these have small diameter and are difficult to patch onto one may have to turn to optical recordings, Meyer *et al.* (1997).

3. **The Nonuniform Active Cable**

We now demonstrate the localization of active channel densities in the presence of a known leak profile. Following Spruston and Stuart we focus on the hyperpolarization activated so called h–current. The cable equation now reads

$$\begin{aligned} G_i v_{xx} &= C_m v_t + G_l(x)(v - E_l) + G_h(x) u^2 (v - E_h) \\ u_t &= F(u,v) \equiv \frac{u_\infty(v) - u}{\tau_u(v)} \end{aligned} \tag{3.1}$$

where u denotes the gating variable for the h–current. Its reversal potential, $E_h = -55\,mV$, is close to rest while its associated steady–steady activation and time constant functionals behave as depicted below.

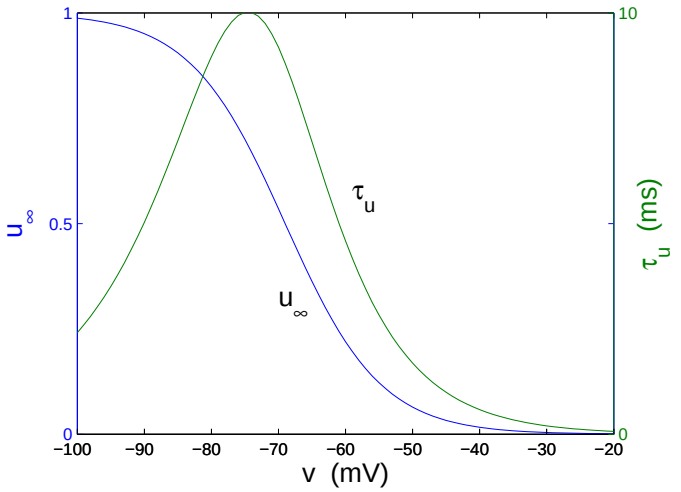

Figure 3. The h–current steady–state activation, $u_\infty(v) = 1/(1 + \exp((v + 69)/7.1))$, and time constant, $\tau_u(v) = 10/(\exp((v + 66.4)/9.3) + \exp(-(v + 81.6)/13))$

We suppose, as in (2.3), that the fiber is driven $x = 0$ and sealed at $x = \ell$. The existence now of 2 distinct and nonuniform conductances compels the rest potential to likewise be nonuniform. In particular,

$$v(x,0) = \overline{v}(x) \quad \text{and} \quad u(x,0) = u_\infty(\overline{v}(x)) \tag{3.2}$$

where $\overline{v}$ satisfies

$$G_i\overline{v}''(x) = G_l(x)(\overline{v}(x) - E_l) + G_h(x)u_\infty^2(\overline{v}(x))(\overline{v}(x) - E_h), \qquad \overline{v}'(0) = \overline{v}'(\ell) = 0. \quad (3.3)$$

This scenario then calls for 4 Lagrange multipliers, 2 to enforce the 2 state equations, (3.1), and 2 to enforce the two initial conditions, (3.2). The full Lagrangian therefore takes the form

$$\begin{aligned} L(G, v, V, u, U, \eta, \zeta) &= \frac{1}{2}\int_0^T \{|v(0,t) - v_0^e(t)|^2 + |v(x_1,t) - v_1^e(t)|^2\}\,dt \\ &+ R_i \int_0^T \int_0^\ell \{C_m v_t - G_i v_{xx} + G_l(x)(v - E_l) + G(x)u^2(v - E_h)\}V\,dx\,dt \\ &+ \int_0^T \int_0^\ell \{u_t - F(u,v)\}U\,dx\,dt + \int_0^\ell \{u(x,0) - u_\infty(v(x,0))\}\zeta(x)\,dx \\ &+ R_i T \int_0^\ell \{G_i v_{xx}(x,0) - G_l(x)(v(x,0) - E_l) - G(x)u^2(x,0)(v(x,0) - E_h)\}\eta(x)\,dx, \end{aligned}$$

where G_l is presumed known and G is the stand–in for the to–be–determined G_h. We may expect that V (and U) will solve the adjoint cable equation, and η (and ζ) will solve the adjoint rest condition, stemming from the critical point conditions $\partial_v L = \partial_u L = 0$. As in the previous section we proceed to differentiate L with respect to each of its variables. The most important of these being

$$\begin{aligned} \langle \partial_G \Phi, \tilde{G}\rangle &= \langle \partial_G L, \tilde{G}\rangle \\ &= R_i \int_0^T \int_0^\ell u^2(v - E_h)V\tilde{G}\,dx\,dt - R_i T \int_0^\ell u^2(x,0)(v(x,0) - E_h)\eta\tilde{G}\,dx. \end{aligned} \quad (3.4)$$

Regarding $\partial_v L$, with $\tilde{v}_x(0,t) = \tilde{v}_x(\ell,t) = 0$, integration by parts reveals

$$\begin{aligned} \langle \partial_v L, \tilde{v}\rangle &= \int_0^T (v(0,t) - v_0^e(t) - (a/2)V_x(0,t))\tilde{v}(0,t)\,dt \\ &+ (a/2)\int_0^T V_x(\ell,t)\tilde{v}(\ell,t)\,dt + R_i C_m \int_0^\ell \tilde{v}(x,T)V(x,T)\,dx \\ &+ R_i \int_0^T \int_0^\ell \{(G_l + Gu^2)V - C_m V_t - G_i V_{xx} - \partial_v F(u,v)U/R_i \\ &\qquad + \delta(x - x_1)(v - v_1^e(t))/R_i\}\tilde{v}\,dx\,dt \\ &+ \int_0^\ell \{R_i T G_i \eta'' - R_i T(G_l + Gu^2(x,0))\eta - u_\infty'(v(x,0))\zeta - R_i C_m V(x,0)\}\tilde{v}(x,0)\,dx \end{aligned}$$

and so V must satisfy the adjoint equation

$$\begin{aligned} -C_m V_t - G_i V_{xx} + (G_l + Gu^2)V &= \partial_v F(u,v)U/R_i + \delta(x - x_1)(v - v_1^e(t))/R_i \\ v_0^e(t) - v(0,t) &= (a/2)V_x(0,t) \\ 0 &= V_x(\ell,t) \\ V(x,T) &= 0. \end{aligned} \quad (3.5)$$

In a similar fashion,

$$\begin{aligned}\langle \partial_u L, \tilde{u}\rangle &= \int_0^T \int_0^\ell R_i 2Gu(v-E_h)V\tilde{u} + \tilde{u}_t U - \partial_u F(u,v)U\tilde{u}\,dx\,dt \\ &\quad - \int_0^\ell \{2R_iTGu(x,0)(v(x,0)-E_h)\eta - \zeta\}\tilde{u}(x,0)\,dx \\ &= \int_0^T \int_0^\ell \{2R_iGu(v-E_h)V - U_t - \partial_u F(u,v)U\}\tilde{u}\,dx\,dt \\ &\quad + \int_0^\ell U(x,T)\tilde{u}(x,T)\,dx - \int_0^\ell \{2R_iTGu(x,0)(v(x,0)-E_h)\eta - \zeta + U(x,0)\}\tilde{u}(x,0)\,dx\end{aligned}$$

and so U obey the adjoint equation

$$U_t = 2R_iGu(v-E_h)V + U/\tau_u(v), \qquad U(x,T) = 0. \tag{3.6}$$

while the multiplier

$$\zeta = 2R_iTGu(x,0)(v(x,0)-E_h)\eta + U(x,0) \tag{3.7}$$

and so η must obey the adjoint rest equation

$$\begin{aligned}G_i\eta'' - \{G_l(x) + G(x)u^2(x,0) + u'_\infty(v(x,0))2G(x)u(x,0)(v(x,0)-E_h)\}\eta \\ = (C_m/T)V(x,0) + u'_\infty(v(x,0))U(x,0)/(R_iT) \\ \eta'(0) = \eta'(\ell) = 0.\end{aligned} \tag{3.8}$$

Although the full adjoint system, (3.5)–(3.8), is significantly more complicated than that of the previous section, it is however a *linear* system in the unknown multipliers even though the original system, (3.1), is nonlinear in v and u. We note that the one new term in (3.8), i.e., u'_∞, is automatically and symbolically generated from the user's specification of u_∞.

As in the previous section these systems are amenable to finite elements in space and backward (linear) Euler discretization in time. These in turn permit a discrete representation, similar to (2.16), of the gradient (3.4). As the details of this process add little to what we have already discussed we shall keep them under wraps and move on to our numerical experiments. The cell geometry and parameters will be as above, (2.18), except that the current stimulus is now a $-0.4\ nA$ pulse for 17 ms and the leakage conductance is

$$G_l(x) = 0.2 + \sqrt{x} \quad mS/cm^2.$$

Our target $h-$conductances will be the sigmoid and the Gaussian,

$$G_h(x) = 2 + \frac{8}{1+\exp((\ell/2-x)/.008)} \quad \text{and} \quad G_h(x) = 2 + 8\exp(-(x-\ell/2)^2/0.001)$$

respectively.

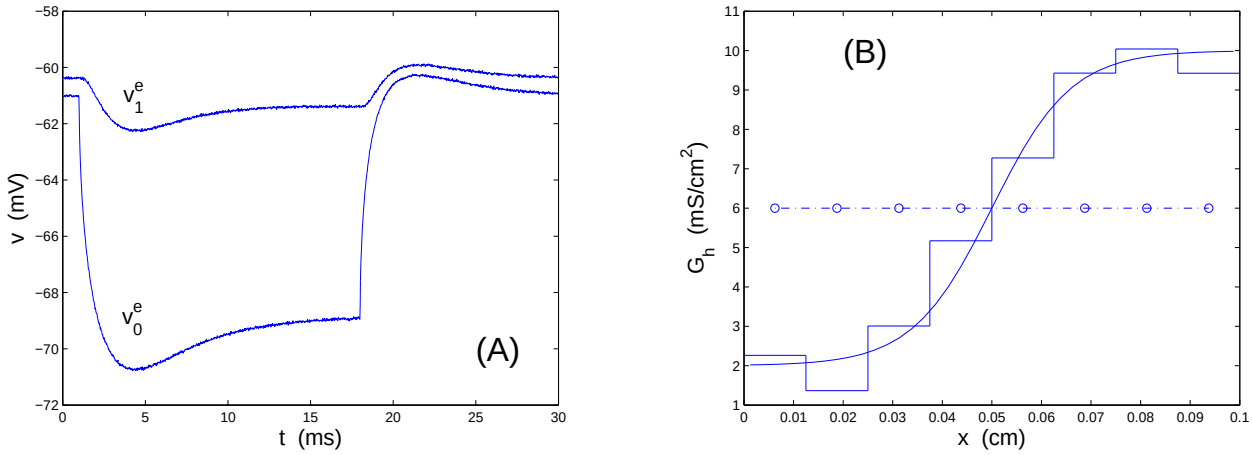

Figure 4. Reconstruction of the sigmoid $h-$conductance. (A) The simulated potential potential recordings at $x = 0$ and $x = x_1$. (B) Exact, initial (o) and recovered (staircase) $h-$conductances using the gradient search routine `fminunc`.

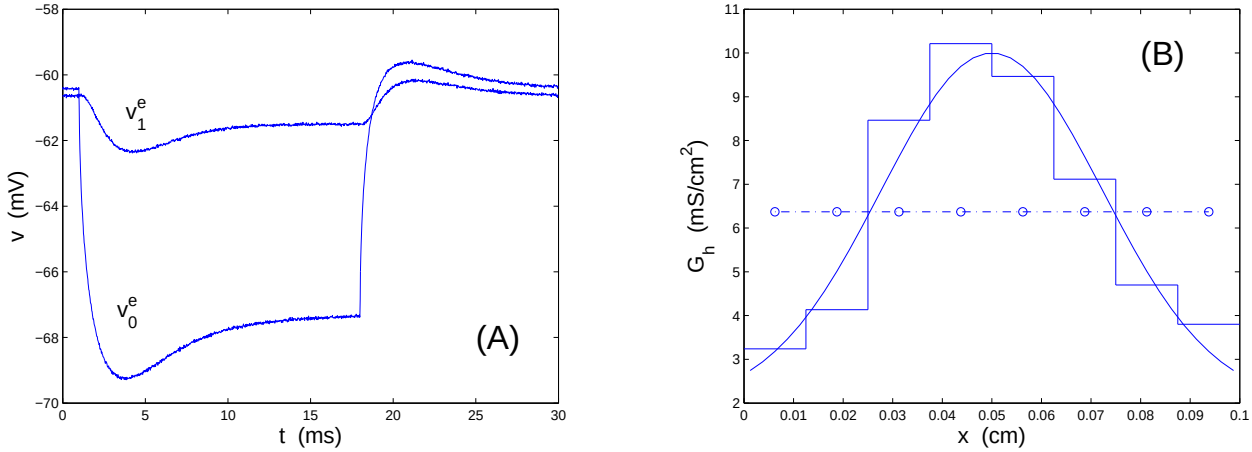

Figure 5. Reconstruction of the Gaussian $h-$conductance. (A) The simulated potential potential recordings at $x = 0$ and $x = x_1$. (B) Exact, initial (o) and recovered (staircase) $h-$conductances using the gradient search routine `fminunc`.

As in the previous section the gradient method outperformed direct search and the incorporation of the analytical gradient, (3.4), resulted in dramatic acceleration.

4. **Discussion**

We have derived an improved means for fitting multi-site voltage recordings to multi–compartment models and successfully tested it on the identification of spatially nonuniform profiles of both leak and h conductances in a straight cable. In order to apply these findings to branched cells one must either (a) assume that each nonuniformity depends only on distance from the soma, or (b) provide voltage recordings from each terminal branch. Application to distribution of other channel types is straightforward. However, application to other channel properties warrants discussion here. The intracellular distribution of

second messengers during learning effects not only open channel conductances but also their kinetics. For example, Magee (1999) observed a shift in the voltage range of activation for h channels with distance from the soma. With respect to figure 3 one might accommodate this shift through

$$u_\infty(v, M(x)) = \frac{1}{1 + \exp((v + M(x))/7.1)}.$$

In this case the gradient of the misfit with respect to the half activation voltage, M, takes the form

$$\begin{aligned}\langle \partial_M \Phi, \tilde{M} \rangle = &- \int_0^T \int_0^\ell \partial_M u_\infty(v(x,t), M(x)) U(x,t) \tilde{M}(x) / \tau_u(v(x,t))\, dx\, dt \\ &- \int_0^\ell \partial_M u_\infty(v(x,0), M(x)) \zeta(x) \tilde{M}(x)\, dx,\end{aligned}$$

and the adjoint system for $\{V, U, \eta, \zeta\}$ remains unchanged, i.e., (3.5)–(3.8). With this one may now execute an effective gradient search for the unknown half activation voltage, M. Such inverse problems have yet to be addressed in the mathematical literature. Beyond the simple question of uniqueness one would also like to suggest to the experimentalist stimulus profile, or profiles, that most accurately and robustly elicits the sought after conductance profile.

5. **References**

Belishev, M.I. (2004), Boundary spectral inverse problem on a class of graphs (trees) by the BC method, Inverse Problems 20: 647–672

Brent, R.P. (2002), Algorithms for Minimization without Derivatives, Dover.

Colbert, C.M., Magee, J.C., Hoffman, D.A., & Johnston, D. (1997) Slow recovery from inactivation of Na+ channels underlies the activity-dependent attenuation of dendritic action potentials in hippocampal CA1 pyramidal neurons, J. Neurosci, 17:6512-6521

Cox, S.J. & Griffith, B. (2001) Recovering Quasi–Active properties of dendrites from dual potential recordings, J. Computational Neuroscience, 11(2):95–110.

Cox, S.J. & Ji, L. (2001) Discerning ionic currents and their kinetics from input impedance data, Bulletin of Mathematical Biology 63(5):909–932.

Daoudal, G. & Debanne, D. (2003), Long-Term Plasticity of Intrinsic Excitability: Learning Rules and Mechanisms Learn. Mem. 10(6):456–465.

Elliott, E.M., Malouf, A.T., Caterall, W.A. (1995) Role of calcium channel subtypes in calcium transients in hippocampal CA3 neurons, J. Neurosci. 15:6433–6444

Hines, M. & Carnevale, N.T. (1997) The NEURON simulation environment, Neural Computation 9, pp. 1179–1209.

Hoffman, D.A., Magee, J.C., Colbert, C.M. & Johnston, D. (1997) K+ channel regulation of signal propagation in dendrites of hippocampal pyramidal neurons, Nature 387:869–75.

Lions, J.L. (1971) The Optimal Control of Systems Governed by Partial Differential Equations, Springer, Berlin.

Lorincz, A., Notomi, T., Tamas, G., Shigemoto, R. & Nusser, Z. (2002) Polarized and compartment-dependent distribution of HCN1 in pyramidal cell dendrites. Nat Neurosci 5(11):1185–93

Magee, J. C. (1998) Dendritic hyperpolarization-activated currents modify the integrative properties of hippocampal CA1 pyramidal neurons. J. Neurosci. 18:7613–7624

Magee, J. C. (1999) Dendritic Ih normalizes temporal summation in hippocampal CA1 neurons. Nat. Neurosci. 2:508–514

Meyer, E., Müller, C.O. & Fromherz, P. (1997) Cable properties of dendrites in hippocampal neurons of the rat mapped by a voltage-sensitive dye. Eur J Neurosci 9(4):778–85

Mickus, T., Jung, H-y., & Spruston, N. (1999) Properties of slow, cumulative sodium channel inactivation in rat hippocampal CA1 pyramidal neurons. Biophys J 76:846-860

Migliore, M., Hoffman, D.A., Magee, J.C., & Johnston, D. (1999) Role of an A-type K+ conductance in the back-propagation of action potentials in the dendrites of hippocampal pyramidal neurons, J. Comp. Neurosci. 7:2-15

Pierce, A. (1979) Unique identification of eigenvalues and coefficients in a parabolic equation, SIAM J. Control and Optimization 17(4):494–499.

Reyes, A. (2001) Influence of dendritic conductances on the input-output properties of neurons, Annu. Rev. Neurosci. 24:653–75

Ross, W.N. & Werman, J.R. (1986) Mapping calcium transients in the dendrites of Purkinje cells from the cerebellum *in vitro*, J. Physiol. (Lond.) 389:319–336.

Sabatini, B. L. & Svoboda, K. (2000) Analysis of calcium channels in single spines using optical fluctuation analysis, Nature. 408:589–593.

Schaefer, A.T., Helmstaedter, M., Sakmann, B. & Korngreen, A. (2003) Correction of conductance measurements in non-space-clamped structures: 1. Voltage-gated K+ channels, Biophys. J. 84:3508–3528

Stuart G & Spruston N (1998) Determinants of voltage attenuation in neocortical pyramidal neuron dendrites, J. Neurosci. 18(10):3501–10

Sugimori, M., Llinás, R., & Anegelides, A., (1986), Flourescence localization of tetrodoxin receptors in mammalian cerebellar cortex *in vitro*, Soc. Neurosci. Abstr. 12:463.

Xu, J., Kang, N., Jiang, L., Nedergaard, M. & J. Kang, (2005), Activity-Dependent Long-Term Potentiation of Intrinsic Excitability in Hippocampal CA1 Pyramidal Neurons, J. Neurosci. 25(7):1750–1760.